Network substrates of cognitive impairment in Alzheimer's Disease

Luke Tait [a,b,c,*], George Stothart [d], Elizabeth Coulthard [e], Jon T. Brown [f], Nina Kazanina [g], Marc Goodfellow [a,h,b,c]

[a] Living Systems Institute, University of Exeter, Exeter, United Kingdom
[b] EPSRC Centre for Predictive Modelling in Healthcare, University of Exeter, Exeter, United Kingdom
[c] College of Engineering, Maths, and Physical Sciences, University of Exeter, Exeter, United Kingdom
[d] Department of Psychology, University of Bath, Bath, United Kingdom
[e] Translational Health Sciences, University of Bristol, Bristol, United Kingdom
[f] University of Exeter Medical School, Exeter, United Kingdom
[g] School of Psychological Science, University of Bristol, Bristol, United Kingdom
[h] Centre for Biomedical Modelling and Analysis, University of Exeter, Exeter, United Kingdom

HIGHLIGHTS

- Cognitive impairment scores correlate with small-worldness of networks in Alzheimer's Disease.
- Computational modelling is used to uncover mechanisms of altered small-worldness.
- Temporal lobe disconnection revealed as a potential mechanism for cognitive impairment.

ABSTRACT

Objectives: Functional and structural disconnection of the brain is a prevailing hypothesis to explain cognitive impairment in Alzheimer's Disease (AD). We aim to understand the link between alterations to networks and cognitive impairment using functional connectivity analysis and modelling.
Methods: EEG was recorded from 21 AD patients and 26 controls, mapped into source space using eLORETA, and functional connectivity was calculated using phase locking factor. The mini-mental state exam (MMSE) was used to assess cognitive impairment. A computational model was used to uncover mechanisms of altered functional connectivity.
Results: Small-worldness (SW) of functional networks decreased in AD and was positively correlated with MMSE score and the language sub-score. Reduced SW was a result of increased path lengths, predominantly localized to the temporal lobes. Combining observed differences in local oscillation frequency with reduced temporal lobe effective connectivity in the model could account for observed functional network differences.
Conclusions: Temporal lobe disconnection plays a key role in cognitive impairment in AD.
Significance: We combine electrophysiology, neuropsychological scores, and computational modelling to provide novel insight into the relationships between the disconnection hypothesis and cognitive decline in AD.

© 2019 International Federation of Clinical Neurophysiology. Published by Elsevier B.V. This is an open access article under the CC BY license (http://creativecommons.org/licenses/by/4.0/).

1. Introduction

Dementia is a neurological disorder that is characterised by progressive cognitive decline; common symptoms in the early stages include memory loss, language impairments, visuospatial impairments and behavioural changes (Agronin, 2014).

Alzheimer's Disease (AD) is the most common disease causing dementia; approximately 70% of dementias have been identified to be caused by AD based on clinical diagnosis and postmortem examination of the brain (Barker et al., 2002; Bermejo-Pareja et al., 2008). One of the key challenges for developing treatment methods for AD is understanding the pathological mechanisms in the brain underlying cognitive impairment.

A prevailing hypothesis for cognitive impairment in AD is the disconnection of distributed neuronal networks such that ability of different processing systems to integrate is compromised

* Corresponding author at: Living Systems Institute, University of Exeter, Exeter, United Kingdom.
E-mail address: Lt349@exeter.ac.uk (L. Tait).

(Delbeuck et al., 2003). Evidence for the disconnection hypothesis comes from a wide range of behavioural, functional, structural, and effective connectivity studies. Structural imaging methods such as diffusion weighted imaging (DWI) and diffusion tensor imaging (DTI) have been used to identify reduced white matter integrity in AD (Rose et al., 2000; Mito et al., 2018), suggestive of long range synaptic disconnection. Although structural connectivity provides a substrate for functional integration, it does not allow for study of dynamic integration of nodes in brain networks (Honey et al., 2009), and therefore cannot fully explain emergent spatiotemporal brain dynamics (Tsang et al., 2017). In order to quantify co-activity between regions of the brain, 'functional networks' can be elucidated from time series data. Disconnection in AD has been identified in functional networks derived from imaging modalities such as EEG (Babiloni et al., 2016), MEG (Stam et al., 2009), functional MRI (Badhwar et al., 2017), and PET (Cope et al., 2018). An advantage of using EEG/MEG is that it is primarily generated by post-synaptic potentials (Olejniczak, 2006) and is therefore more directly linked to neuronal activity than other functional imaging modalities such as functional MRI which tracks haemodynamic response to neuronal activity and thus operates on a much slower time scale (Crosson et al., 2010). Because of this high temporal resolution, EEG is able to shed light on disruptions to local dynamics such as slowing of neuronal oscillations in AD (Brueggen et al., 2017).

To bridge the gap between synchronized neuronal activity and synaptic connectivity, 'effective connectivity' studies combine computational models with both structural and functional imaging to elucidate how changes in both intrinsic dynamics and structural connectivity alter functional networks. In AD, effective connectivity studies have been used to relate structural and functional disconnection (Dermitas et al., 2017; de Haan et al., 2012), further supporting the disconnection hypothesis of AD. However, it is unclear whether observations of functional disconnection could be explained by alterations to local dynamics, such as observed in AD patients (Brueggen et al., 2017).

Intuitively, disconnection would lead to an impaired ability of brain regions to exchange information (Uhlhaas and Singer, 2006). However, the exact links between specific disruptions to connectivity and resulting cognitive deficits of AD have not been well characterised. Cognitive function can be quantified in dementia clinics via the mini-mental state examination (MMSE) (Folstein et al., 1975). The MMSE includes tests of cognitive abilities such as spatial and temporal orientation, attention, memory, language, recall, and motor skills, giving scores for ability in each area. A number of studies have correlated structural and functional disconnection with cognitive test scores in AD patients, typically focusing on global network properties and the total MMSE score (Wu et al., 2011; Stam et al., 2007; Lo et al., 2010; de Hann et al., 2009). However, MMSE is a broad cognitive screen probing memory, language and visuospatial function, each of which are thought to depend on distinct neuroanatomical circuitry. A quantitative link between specific network deficits and individual cognitive domains might yield more precise information about the mechanisms of cognitive decline in AD, and therefore potentially inform treatment.

Here, we study functional connectivity derived from the EEG of AD patients and healthy controls, and examine the relationship between network topology and cognitive ability. We hypothesise that in AD, specific alterations to functional networks will correlate with impairments in particular cognitive domains due to disruption of integration between brain areas related to these domains, in line with the disconnection hypothesis of AD. To test this hypothesis, local and global properties of the functional networks are quantified and correlated with MMSE subscores. To provide validation that alterations to functional networks are a result of alterations to the structural connectome and not due to alterations to distributed heterogeneity in the intrinsic node dynamics, we use a computational model which reflects realistic changes in the frequency spectrum observed in the data. Our results give crucial insight into the role of functional and effective disconnection in deterioration of ability in specific cognitive domains in AD. Since patients in the study were free from medication, our results provide a valuable diagnostic biomarker of Alzheimer's Disease that are not attributable to effects of medication.

2. Materials and methods

2.1. EEG collection and preprocessing

All appropriate approvals for our procedures were obtained from the National Research Ethics Service Committee South West Bristol (Ref. 09/H0106/90). Participants provided written informed consent before participating and were free to withdraw at any time. AD patients were recruited from memory clinics in the South West of England on a consecutive incident patient basis. The diagnosis of AD was determined by clinical staff using neurological, neuroimaging, physical and biochemical examination together with the results of family interview, neuropsychological and daily living skills assessment according to DSM-IV (American Psychiatric Association, 2000) and NINCDS-ADRDA guidelines (McKhann et al., 1984). All patients were free from any medication known to affect cognition, e.g. cholinergic medications prescribed to treat dementia symptoms, anti-psychotics, anti-depressants, benzodiazepines, Warfarin, etc. The HOA control group was recruited from the memory clinics' volunteer research panels and were in normal general health and had no evidence of a dementing or other neuropsychological disorder, according to NINCDS-ADRDA guidelines (McKhann et al., 1984). Exclusion criteria for all groups included poor general health or a history of transient ischemic attack or stroke, significant head injury and any other significant psychiatric disorder or neurological disease. Data on subjects is given in Tables 1 and 2.

Resting-state, eyes open EEG (64 channel) was recorded from all subjects prior to the beginning of a battery of cognitive tasks. This period, and the subsequent battery of tasks, were consistent across the two groups. A single 20 s epoch of EEG, sampled at 1 kHz, was extracted per subject. Independent component analysis was used to remove visual and cardiac artifacts. There were no significant differences in the number of artifacts removed between HOA and AD (HOA: 3.69 ± 0.46, range 0–10; AD: 4.09 ± 0.42, range 1–8; $p = 0.4747$, Mann Whitney U-test). Line noise at 50 Hz was removed and replaced by linear interpolation of the power spectrum. Data was bandpass filtered at 1–200 Hz, demeaned, slow non-physiological trends up to third order polynomials removed, and re-referenced to average. These preprocessing steps were performed using the Fieldtrip toolbox for EEG/MEG-analysis, developed at the Donders Institute for Brain, Cognition and Behaviour (Oostenveld et al. (2011); http://www.ru.nl/neuroimaging/fieldtrip). Example EEG time series are shown in Fig. S1.

Table 1
Data for healthy older adults and Alzheimer's Disease subjects.

	HOA	AD
Age ($\pm$ SEM; years)	76 ($\pm$ 7)	79 ($\pm$ 9)
MMSE ($\pm$ SEM)	29 ($\pm$ 1)	23 ($\pm$ 3)
n	26	21
Male	14	8
Female	12	13

Table 2
Mini-mental state examination subscores for healthy older adults and Alzheimer's Disease subjects.

	HOA	AD
Orientation to time	4.83 (± 0.41)	3.19 (± 1.42)
Orientation to place	5.00 (± 0.00)	4.13 (± 0.72)
Immediate recall	3.00 (± 0.00)	2.94 (± 0.25)
Serial 7s	4.83 (± 0.41)	3.75 (± 1.61)
World backwards	5.00 (± 0.00)	4.81 (± 0.40)
Registration recall	2.67 (± 0.52)	0.44 (± 0.81)
Language	7.83 (± 0.41)	6.44 (± 1.09)
Pentagons	1.00 (± 0.00)	0.81 (± 0.40)
n	6	16

2.2. Source reconstruction

Source reconstruction was performed using the Fieldtrip toolbox (Oostenveld et al. (2011); http://www.ru.nl/neuroimaging/fieldtrip). A template 3 layer boundary element method volume conduction model (Oostenveld et al., 2003) was used in conjunction with a template cortical source model consisting of 5124 point sources on a canonical cortical surface taken from Statistical Parameter Mapping 8 (SPM8; https://www.fil.ion.ucl.ac.uk/spm/software/spm8/) and implemented in Fieldtrip. Use of template models has previously been demonstrated to perform well compared to individual models derived from MRI (Fuchs et al., 2002). Dipoles were oriented normal to the surface of the cortical sheet (Hassan et al., 2014). Fig. 1 shows the template model.

Exact low resolution brain electromagnetic tomography (eLORETA) was used to solve the inverse problem and reconstruct source activity at each of the 5124 source points (Pascual-Marqui, 2007; Pascual-Marqui, 2009). eLORETA is a linear, regularized, weighted minimum norm inverse solution with theoretically exact, zero error localization even in the presence of structured biological or measurement noise (Pascual-Marqui, 2007), is suited to the study of whole brain phase synchronization (Pascual-Marqui et al., 2011; Finger et al., 2016), and the LORETA family of solutions have been validated against numerous imaging modalities (Dierks et al., 2000; Vitacco et al., 2002; Mulert et al., 2004; Pizzagalli et al., 2004; Zumsteg et al., 2005, 2006; Olbrich et al., 2009) and simulations (Pascual-Marqui et al., 2011; Finger et al., 2016).

2.3. Power spectral analysis

All power spectra were extracted by computing the Fourier transform of the data. The five frequency bands of interest are given in Table 3 (Buzsaki, 2006), whilst the broadband was defined as 1–45 Hz as this encompasses the range of these bands. Total power in a band $[f_1, f_2]$ was computed as $\sum_{f \in [f_1, f_2]} P(f) \Delta f$, where $P(f)$ is the power at frequency f and Δf is the frequency resolution of the data. The *relative power* spectrum (Wang et al., 2015) is defined as the power spectrum normalized by total broadband power and acts as a probability distribution over frequencies, i.e. the relative power at a given frequency is the contribution of that frequency to the overall power.

In order to calculate the peak frequency of a spectrum $P(f)$ in a band $f \in [f_1, f_2]$, the spectrum was smoothed with a moving average filter of order 1 Hz (20 frequency points in this data). Peaks of the spectrum with widths at half prominence greater than 0.5 Hz were then extracted. These steps reduced the likelihood that peaks were due to noise in the spectrum. The peak frequency was then the extracted peak with maximum amplitude within the band of interest (Klimesch, 1999).
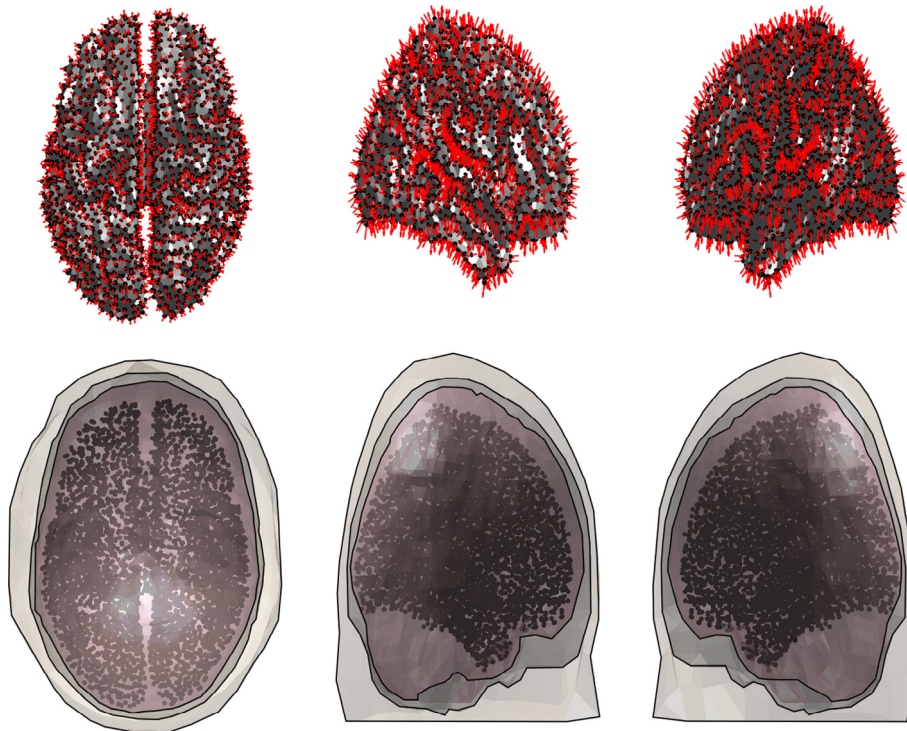

Fig. 1. Template head model used for source reconstruction. (Top) Template cortical surface is shown in grey. Black dots represent source points distributed along the surface. Red arrows show dipole orientation, normal to the surface. (Bottom) Template boundary element method volume conduction model. Black dots are the same as those shown in the top row of figures, representing source points. Pink (inner layer) is conductive brain tissue. Dark grey (middle layer) is skull tissue, and light grey (outer layer) is flesh. (For interpretation of the references to colour in this figure legend, the reader is referred to the web version of this article.)

Table 3
Frequency bands used in the analysis. For each band, a Mann Whitney U test was performed on relative power within that band, testing AD vs HOA (see Section 3.1). *p*-values reported are Bonferroni corrected for multiply hypothesis. Superscript * denotes significance to *p*<0.05.

Band name	Frequency range [Hz]	Relative Power *p*-value AD vs. HOA
δ	1–4	0.6849
θ	4–8	0.0187[*]
α	8–13	0.8052
β	13–30	0.4446
γ	30–45	0.5310

2.4. Functional connectivity analysis

To build functional networks, source reconstructed data was parcellated into 40 regions of interest (ROIs) based on the Brainnetome atlas (Fan et al. (2016); http://atlas.brainnetome.org/). A list of ROIs is given in Table 4. The Brainnetome atlas contains 48 regions of the brain; however, source points were restricted to the cortical surface and hence the 8 subcortical nuclei (amygdala, hippocampus, basal ganglia, and thalamus in the left and right hemispheres) were omitted.

Parcellation was performed by taking the first principal component of all source points within a given ROI in order to construct a single time series for that ROI (Hassan and Wendling, 2018). For eLORETA solutions, which constrain spatial smoothness and are low resolution, the activity of local voxels is highly correlated. The time course of the first principal component of all voxels in the ROI is a single time series whose value at each time point is minimally different to the activity of all voxels, i.e. it maximises the spatial variance explained. Functional networks were constructed by calculating the phase locking factor (PLF) (Lachaux et al., 1999) between pairs of ROI time series. PLF between ROIs *i* and *j* is given by

$$c_{ij} = \frac{1}{T}\left|\sum_{k=1}^{T} e^{i\Delta\phi_{ij}(k)}\right|, \tag{1}$$

where *T* is the number of sampling points in the 20 s segment of data and $\Delta\phi_{ij}(k)$ is the difference between the instantaneous phases of signals *i* and *j* at sampling point *k*. Instantaneous phases were calculated by taking the angle of the Hilbert transform of the signal. PLF was calculated using custom written routines using MATLAB R2017b (www.mathworks.com).

To test edges against the null hypothesis that functional connections are due only to power spectral composition and distribution, each edge was tested to 5% significance vs 99 iterative amplitude adjusted Fourier transform surrogates (Schreiber and Schmitz, 1996). Due to the low resolution nature of eLORETA and therefore the potential for source leakage, there is the possibility that during the parcellation procedure common signals may be parcellated into more than one region, resulting in a spurious phase relationship between the signals (Pascual-Marqui et al., 2011). Since this phase relationship will manifest as a zero lag connection (Pascual-Marqui et al., 2011), PLF values with zero phase lag connection were set to zero. Furthermore, spurious indirect functional connections may arise due to strong indirect connections. For example, if node A strongly influences both node B and node C, we might observe a functional connection between nodes B and C due to common drive. Therefore, edges between pairs of nodes for which there existed a shorter indirect path were set to zero (Schmidt et al., 2014). The shortest path between nodes was calculated using the Dijkstra algorithm (Dijkstra, 1959), where the symmetric, direct distance between nodes *i* and *j* is given by $1/c_{ij}$.

2.5. Graph theoretical measures

To quantify properties of the functional network structure, a number of graph theoretical measures were used. These measures are outlined below. In the following section, *N* is the number of nodes in the network, and the matrix *C* is the weighted adjacency matrix where element c_{ij} is the PLF value (corrected for surrogates, zero phase lag, and indirect corrections) between ROIs *i* and *j*.

The *degree* of node *i* is the sum of weighted connections of the node (Rubinov and Sporns, 2010), given by

$$d(i) = \sum_{j\neq i} c_{ij}. \tag{2}$$

The *mean degree* of the network is then given by

$$MD = \frac{1}{N}\sum_{i=1}^{N} d(i), \tag{3}$$

and is a global measure of how synchronous the network is on average. The mean degree gives no information on the topological structure of the network, so a number of other graph theoretical measures can be used to further quantify topology. Since many topological measures are sensitive to changes in average synchrony with no changes in topology (e.g. by multiplying each edge by a

Table 4
ROIs for parcellation of source data. N is the number of source points from the 5124 original cortical sources within the ROI, and the label left/right represents hemisphere.

ROI	N (right)	N (left)	ROI	N (right)	N (left)
Frontal lobe					
Superior frontal gyrus	174	168	Medial frontal gyrus	188	158
Inferior frontal gyrus	76	77	Orbital gyrus	171	160
Precentral gyrus	168	133	Paracentral gyrus	37	40
Temporal lobe					
Superior temporal gyrus	142	85	Middle temporal gyrus	71	91
Inferior temporal gyrus	90	87	Fusiform gyrus	108	102
Parahippocampal gyrus	96	91	Posterior superior temporal sulcus	40	34
Parietal Lobe					
Superior parietal lobule	107	100	Inferior parietal lobule	285	301
Precuneus	116	126	Postcentral gyrus	152	131
Occipital lobe					
Medioventral occipital cortex	125	168	Lateral occipital cortex	132	196
Others					
Insular gyrus	86	89	Cingulate gyrus	199	224

constant), we first define matrix A with elements $a_{ij} = c_{ij}/\text{MD}$. As a measure of network topology, we quantified small-worldness.

A 'small-world' network is characterised by two key features; neighbours of a node are likely to also be neighbours, and no two nodes have a long path length between them (Watts and Strogatz, 1998; Humphries and Gurney, 2008). The *small-worldness* of a network (Humphries and Gurney, 2008) is therefore given by

$$\text{SW} = \frac{(C/C_0)}{(L/L_0)}, \qquad (4)$$

where C is the clustering coefficient of the network and C_0 is the clustering coefficient of a random network of equal average synchrony and distribution of edges (estimated by generating 10 networks with randomly rewired edges), where clustering coefficient is given by Rubinov and Sporns (2010)

$$C = \frac{\sum_{i=1}^{N}\sum_{j\neq i}\sum_{k\neq i,j}\left(a_{ij}a_{ik}a_{jh}\right)^{1/3}}{\sum_{i=1}^{N}\kappa_i(\kappa_i - 1)}, \qquad (5)$$

which is the probability that given two nodes j and k are neighbours of node i, nodes j and k are neighbours of each other (weighted by strengths of edges). Here, κ_i is the number of connections made by node i. Furthermore in Eq. (4) L is the characteristic path length of the network (and L_0 is the characteristic path length of the random network), where characteristic path length is given by Rubinov and Sporns (2010)

$$L = \frac{1}{N(N-1)}\sum_{i=1}^{N}\sum_{j=1}^{N}\delta_{ij}. \qquad (6)$$

Here, δ_{ij} is the path length between nodes i and j, and is calculated using the Dijkstra algorithm (Dijkstra, 1959). Finally, a measure that acts as a local counterpart to the (reciprocal of) characteristic path length is the *closeness centrality* of a node (Rubinov and Sporns, 2010), given by

$$\ell(i) = \frac{N-1}{\sum_{j\neq i}\delta_{ij}}. \qquad (7)$$

It can be seen from Eqs. (6) and (7) that characteristic path length is the average of the reciprocal of closeness of all nodes in the network.

2.6. Computational model

We used a phenomenological model based on that of Dermitas et al. (2017). Each of the 40 ROIs described in Table 4 was modelled using the normal form of a supercritical Hopf bifurcation, with the dynamics of ROI i given by

$$\dot{v}_i = \left(a - v_i^2 - u_i^2\right)v_i - \omega_i u_i + G\sum_{j\neq i}K_{ij}\left(v_j - v_i\right) + \sigma\eta_i(t) \qquad (8)$$

$$\dot{u}_i = \left(a - v_i^2 - u_i^2\right)u_i + \omega_i v_i, \qquad (9)$$

where v_i is the current density of node i and u_i is a recovery variable, whilst a, ω_i, G and K_{ij} are parameters described below. G is a global connectivity parameter, set to $G = 1$ unless otherwise stated. The term $\sigma\eta_i(t)$ is a noise term, where $\sigma = 0.02$ (Dermitas et al., 2017) is the variance of the noise and $\langle\eta_i(t)\rangle = 0$ and $\langle\eta_i(t),\eta_i(s)\rangle = \delta(t-s)$.

When the bifurcation parameter a is negative, the uncoupled deterministic system (with $\sigma = 0$ and $K_{ij} = 0\forall(i,j)$) is a focus steady state with natural frequency ω_i. At $a = 0$, a bifurcation occurs so that when a is positive the system is in a stable periodic orbit with frequency ω_i. Here, we used $a = -0.05$ as Dermitas et al.

(2017) found this gave the best fit to empirical functional connectivity matrices.

We optimized the effective connectivity matrix K such that the simulated functional connectivity recreated target empirical functional connectivity using a simple procedure based on that of Dermitas et al. (2017). Our target empirical functional connectivity matrix was the median of all HOA functional connectivity matrices. The optimization was performed by setting the natural frequency for each node, ω_i, to the corresponding median peak frequency for each ROI in HOA subjects. The effective connectivity was initialized with $K_{ij} = 1$ if there exists some anatomical connection between ROIs i and j and $K_{ij} = 0$ otherwise, based on template structural imaging data from the Brainnetome atlas (Fan et al. (2016); http://atlas.brainnetome.org/). An iterative algorithm was used to optimize the weights on this matrix, where the effective connectivity at iteration n is given by

$$K_{ij}[n] = K_{ij}[n-1] + 0.2\left(c_{ij}^{\text{emp}} - c_{ij}^{\text{sim}}[n-1]\right), \qquad (10)$$

where c_{ij}^{emp} is the target empirical functional connectivity, whilst $c_{ij}^{\text{sim}}[n]$ is the simulated functional connectivity at iteration n.

To choose an optimum matrix K, an error function was defined as $\text{Error}[n] = 1 - r(c^{\text{sim}}[n], c^{\text{emp}})$, where $r(A, B)$ is the correlation of the edges of functional connectivity matrices A and B. Due to the stochastic nature of the Hopf simulations resulting in noise on the error, instead of choosing the iteration with minimum error as optimum (Dermitas et al., 2017), we apply a moving average filter of order 25 iterations to the error function and select the minimum of this. Effective connectivity is chosen as the mean effective connectivity of the 25 iterations averaged over at the minimum.

During all subject specific simulations, the effective connectivity matrix remained at this value unless otherwise stated. Natural frequencies of the oscillators were the individual subject's peak power spectral frequencies. In simulations for which global connectivity G was optimized, Matlab's fzero function (https://www.mathworks.com/help/matlab/ref/fzero.html) was used with the difference between the empirical and simulated mean degrees as the error function.

2.7. Statistical analysis

All p-values reported here were computing using the Mann-Whitney U-test, which is non-parametric and therefore makes no assumptions about the distribution of the data. Families of tests were corrected for multiple hypotheses using the Bonferroni correction - specifically, p-values were multiplied by the number of hypotheses being corrected for. Significant results were those with Bonferroni adjusted p-values less than 0.05. Effect sizes for the Mann-Whitney U-test are given by the rank biserial correlation (Cureton, 1956; Wendt, 1972), which is equivalent to the Mann-Whitney U statistic normalized between zero and one, given by

$$\overline{U} = 1 - \frac{2U}{n_1 n_2}, \qquad (11)$$

where $\overline{U}$ is the rank biserial correlation, U is the U-statistic, and n_i is the number of patients in cohort i. To help interpret this measure, we can consider an alternative (but equivalent) formulation of rank biserial correlation. If we make some hypothesis on the statistic being tested (e.g. the statistic will be larger for HOA than AD), then take all pairs of AD and HOA subjects, rank biserial correlation is the absolute value of the fraction of pairs that support the hypothesis (in our example, pairs where the statistic is larger for the HOA subject than the AD subject) minus the fraction that are against the hypothesis (pairs where AD is larger than HOA). If all pairs support

or all pairs are against the hypothesis (large effect size), $\overline{U} = 1$, whilst if an equal number are for and against (no effect size), $\overline{U} = 0$.

3. Results

3.1. Global power spectrum and functional connectivity analysis

As a first step, we aimed to characterise changes in dynamics and functional networks in AD patients, relative to healthy older adults. To do this, EEG from HOA and AD patients was projected into source space using eLORETA and downsampled to 40 ROIs (Table 4), see Methods. Table 1 contains subject information. To investigate potential slowing of the EEG in AD patients (Strik et al., 1997; Adler et al., 2003; Lindau et al., 2003; Dauwels et al., 2011; Hatz et al., 2015; Liu et al., 2015; Wang et al., 2015; Goossens et al., 2017), we calculated the power spectrum of the EEG for each subject, averaged over all ROIs. There was no significant difference in total broadband (1–45 Hz) power between AD and HOA patients ($p = 0.3745$). To explore the contributions of different rhythms to the overall EEG, we calculated the relative power spectrum averaged over all ROIs (Fig. 2A). It can be seen that slower frequencies, between around 3 and 10 Hz, are more prominent in the AD patients than the HOA. Furthermore, faster frequencies (above around 15 Hz) are less prominent in the AD patients, suggesting a slowing of the EEG in AD. To further quantify these observations, we calculated total relative power in each of the five classic frequency bands, given in Table 3, Fig. 2B). Delta, theta and alpha relative power was found to increase on average in AD patients, whilst beta and gamma rhythms decreased on average. However, the only significant difference was the increase in theta relative power (θRP) ($p = 0.0187$; see Table 3 for p-values in other bands.) For this reason, we focused our remaining analysis on the theta band. Fig. 2C-D show spatial distributions and effect sizes

for changes in theta power, suggesting that the observed slowing of the EEG is predominantly driven by the frontal and parietal lobes.

We extended this analysis into the spatial domain by constructing theta band functional networks, calculating the phase locking factor (PLF; Eq. (1)) between the activity of each pair of ROIs. To quantify average synchrony in the network, mean degree (MD; Rubinov and Sporns (2010)) was calculated. To complement this, we used small-worldness (SW; Humphries and Gurney (2008)) as a quantification of topological organization of the networks. MD was found to increase significantly ($p = 0.0111$) in AD patients, suggesting the presence of enhanced synchrony on average in AD. However, SW was found to decrease significantly ($p = 0.0318$) in AD patients, suggesting that the topology of the network AD networks are organized less efficiently for information transfer (Latora and Marchiori, 2001). Fig. 3 shows boxplots of each of these measures for HOA vs AD.

3.2. Relationships between functional network measures and cognition

The relationship between specific changes to functional networks in AD and the phenotype of the disease is not well understood. To investigate this, we calculated the correlation between spectral and functional network measures and cognitive test scores. 20 out of the 21 AD subjects we analysed undertook the mini mental state examination (MMSE), which provides a score out of 30 based on cognitive tasks (Folstein et al., 1975). Average scores for both the HOA and AD cohorts are given in Table 1.

The Pearson's correlation between MMSE score and each of the measures (θRP, MD, SW) was calculated. The only measure that exhibited a significant correlation with MMSE score was SW ($r = 0.5921$, $p = 0.0060$) (Fig. 4), suggesting that functional network topology is associated with cognitive decline in AD. A full list of correlations and p-values can be found in Table S1.
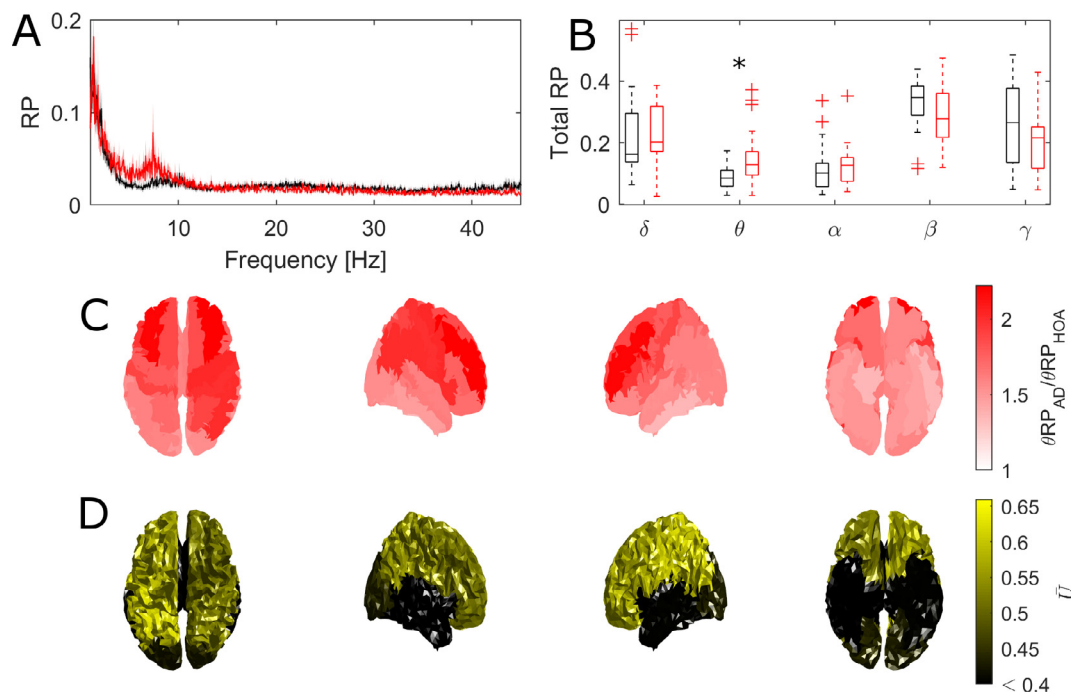

Fig. 2. **Power spectral analysis**. (A) Average relative power over all ROIs. The black line is HOA, and the red is AD. Shaded regions are standard error on the mean. (B) Boxplots of total relative power in each frequency band. Black boxes are HOA, red is AD. The only significant change in AD is the increase in the θ (4–8 Hz) band. (C) Ratio of the within-group mean θ relative power in AD vs HOA for each ROI shows an increase over all ROIs. (D) Effect size of increase in θ relative power for each lobe (see Table 4). Frontal and parietal lobes in both hemispheres were significant to $p < 0.05$ after Bonferonni adjustment of p-values. In C and D, views are (from left to right) top down with subject facing towards top of page, right hemisphere, left hemisphere and from underneath looking up with subject facing towa.rds top of page. (For interpretation of the references to colour in this figure legend, the reader is referred to the web version of this article.)
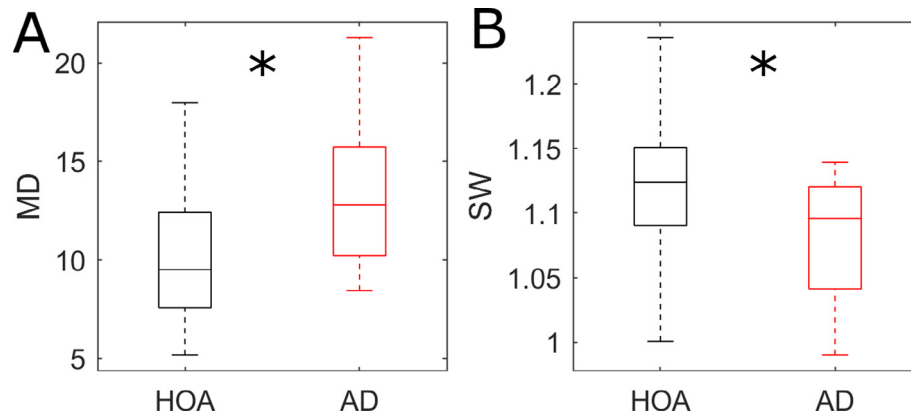
Fig. 3. Global graph theoretical measures for θ band networks. In all cases, black is HOA and red is AD. (A) Mean degree increases significantly in AD. (B) Small-worldness decreases significantly in AD. A star denotes significance (Bonferroni corrected $p < 0.05$).
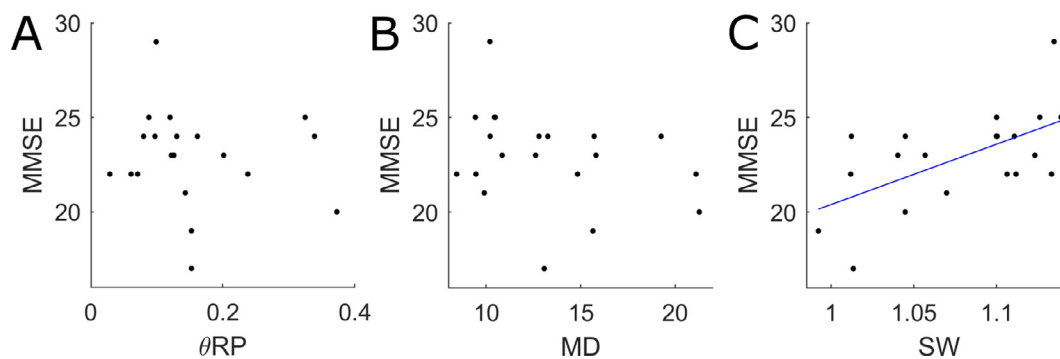

Fig. 4. Correlation between MMSE score and global EEG measures. Plots of MMSE score against (A) theta band relative power, (B) mean degree, (C) small-worldness. Each black dot represents a single patient. Blue lines show linear model fit in the case of significant correlation. (For interpretation of the references to colour in this figure legend, the reader is referred to the web version of this article.)

To develop a deeper understanding of the relationship between functional network topology and cognitive deficits in AD, we tested whether small-worldness correlates with particular aspects of cognition using the MMSE subscores, which were available for 16 of the 21 AD patients (the missing subscores were due to some recruiting clinics only provided total MMSE score). Subscores were orientation to time, orientation to place, immediate recall, attention, memory, language, and drawing overlapping pentagons. Fig. S2 shows boxplots of patient scores for each of these subscores. There was almost no variance in the 16 subjects for orientation to place, immediate recall, memory, or pentagons; for this reason we ruled these subscores out of further analysis. We therefore calculated the correlation of orientation to time, attention (by serial 7s), and language with small-worldness. Of these three subscores, only language was significantly correlated with small-worldness ($r = 0.6132, p = 0.0115$), suggesting that changes to the topology of the functional networks in AD is more predominantly associated with language deficits than attention or orientation to time. Table S2 and Fig. 5 show correlations and p-values of each of these subscores against small-worldness.

3.3. Local topology changes influence small-worldness

In order to add insight into how the pathology of AD relates to behaviour, we sought to further understand how the changes in small-worldness that are associated with language deficits arise in AD. We therefore examined the causes of the observed changes in small-worldness at the level of nodes of the functional networks.

Small-worldness is defined as the ratio of clustering coefficient to characteristic path length (Humphries and Gurney, 2008). To understand whether reduced small-worldness in AD is due to a reduction in clustering coefficient, increased characteristic path length, or both, we quantified each of these measures for the networks. Clustering coefficient demonstrated a small but non-significant decrease in AD ($p = 0.1223$), whilst characteristic path length significantly increased ($p = 0.0303$), suggesting that changes to small-worldness are primarily driven by larger path lengths in the functional network. To identify whether this is a global effect or whether it is driven by certain regions of the brain, we calculated the closeness centrality for each node, which can be interpreted as a local counterpart to (inverse) characteristic path length. That is, nodes with small closeness contribute to a larger characteristic path length.

On average, closeness centrality was found to decrease in all ROIs (Fig. 6A). To gain understanding at the higher level of organisation of lobes of the brain, we averaged closeness centrality into eight lobes (left and right frontal, temporal, parietal, and occipital lobes), and then compared the resulting measure in AD vs HOA for each lobe, via non-parametric statistical testing (Mann-Whitney U test). Effect sizes for the Mann-Whitney U test (quantified by the rank biserial correlation (Cureton, 1956; Wendt, 1972)) for each lobe are shown in Fig. 6B. After Bonferroni correction for multiple hypotheses, only the closeness of the right temporal lobe is significantly different for AD vs HOA (Bonferroni adjusted $p = 0.0343$). However, the effect size for the left temporal lobe is also high (Bonferroni adjusted $p = 0.0579$), and we note that Bonferroni correction is highly conservative, carrying increased
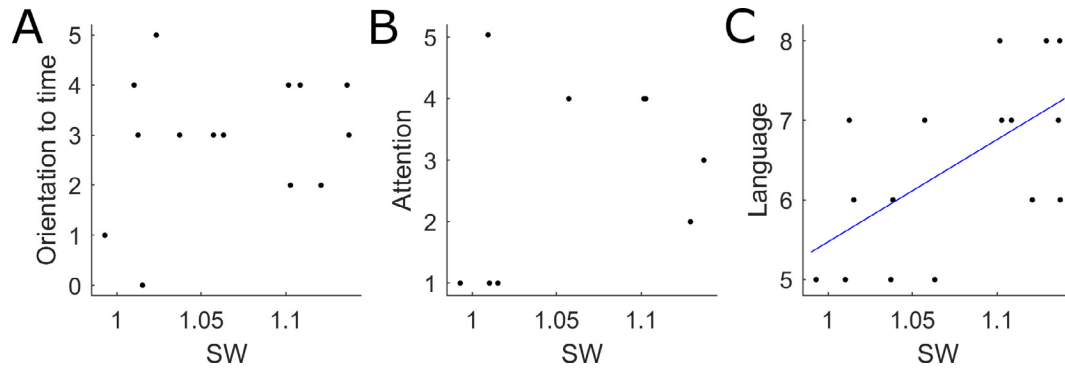
Fig. 5. Correlation between MMSE subscores and small-worldness. Plots of theta band small-worldness against orientation to time (A), attention by serial 7s (B), and language (C) for the AD patients. Each black dot represents a single patient. Blue lines show linear model fit in the case of significant correlation. (For interpretation of the references to colour in this figure legend, the reader is referred to the web version of this article.)
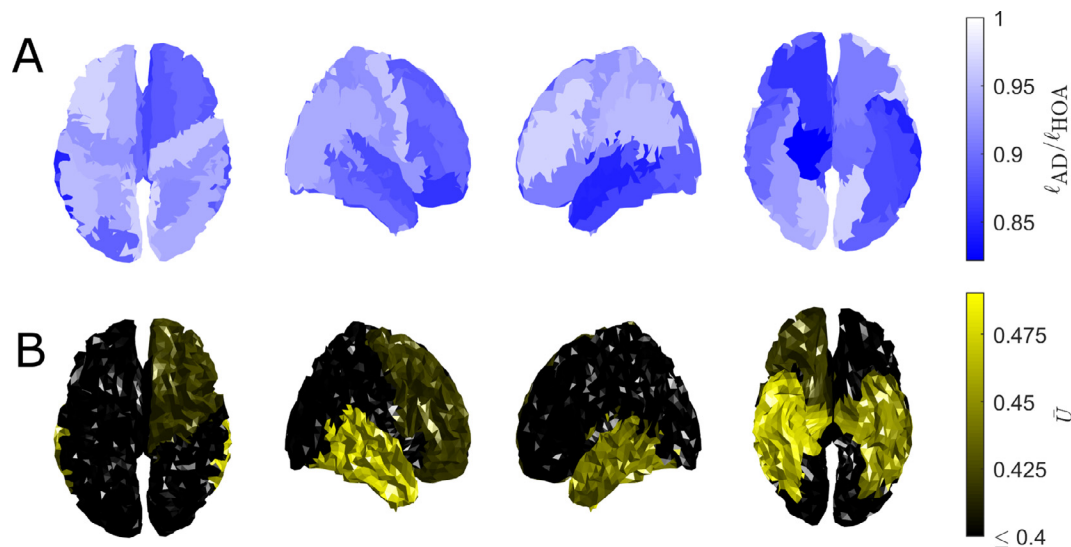

Fig. 6. Closeness centrality of ROIs in theta band networks Decreases in closeness are likely to drive reduced small-worldness in AD. Here, we show (A) the ratio of within-group mean θ closeness in AD vs HOA for each ROI shows a decrease in all ROIs, and (B) effect sizes for each lobe. Effect sizes are largest in the temporal lobes, with the right temporal lobe being significant to $p < 0.05$ after Bonferroni adjustment. For the left temporal lobe, $p = 0.0579$.

chance of type II errors (false negatives) (Perneger, 1998). Fig. 6 and Table S3 demonstrate that the temporal lobes both have a much larger effect size than the rest of the brain. We therefore suggest that it is likely that path length increases in both temporal lobes drive the increased small-worldness in AD.

3.4. Modelling the mechanisms of changes to functional connectivity

In order to better understand the dynamic and network mechanisms that underpin the observed changes to functional connectivity in AD, we used a computational model to simulate brain activity across the ROIs. Fig. 2C-D demonstrated heterogeneous slowing of the power spectrum across ROIs in HOA and AD. Since the distribution of intrinsic frequencies of coupled oscillators plays a vital role in phase locking (Gambuzza et al., 2016; Stam et al., 2007; Lowet et al., 2017), we sought to uncover whether these distributed local power spectral changes alone could account for the observed changes in functional connectivity. To do this, a computational model of coupled stochastically driven oscillators (each representing an ROI) was simulated (see Section 2.6). In the model, spatially heterogeneous alterations to the power spectrum were incorporated via the intrinsic natural frequencies of the oscillators, which are free parameters of the model. For each subject, the

intrinsic frequency of each oscillator was inferred from the data by computing the frequency of the power spectral peak in the 6–13 Hz alpha-theta band for its respective ROI (see Section 2.6). Coupling between oscillators was represented by an effective connectivity (EC) matrix. To focus on the consequences of changes to node frequencies, a representative HOA EC was computed using the median natural frequency distribution for HOA for local dynamics and the median HOA FC as the optimization target (see Section 2.6). Using this EC matrix for all subjects, but individual distributions of frequencies across nodes, we then simulated the model for each subject and examined whether the model revealed differences in FC across cohorts. This method is outlined in Fig. 7.

Fig. S3 shows the simulated networks for all 47 subjects, and Fig. 8A shows an analysis of mean degrees for HOA and AD. The mean degree of the simulated AD networks was significantly larger than in the HOA networks ($p = 0.0152$), suggesting that power spectral slowing may be responsible for the observed increased mean degree in the AD networks. However, the effect size for this increase was notably larger in simulations than in the data. In order to correct this, the global coupling constant in the model was adjusted for each subject until the mean degree of the simulated functional networks matched the mean degree of the empirical functional networks. Fig. S4 shows the simulated networks for
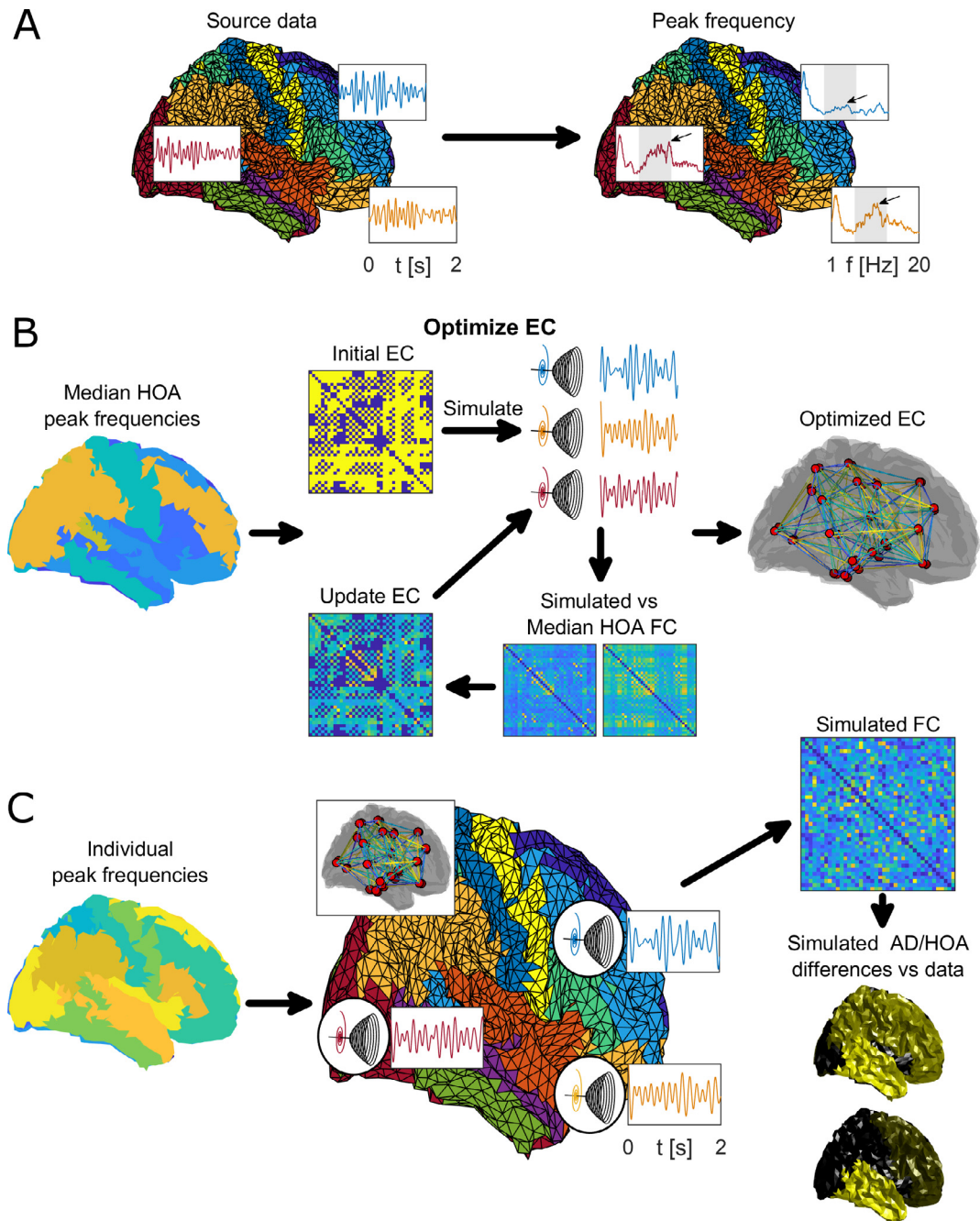
Fig. 7. Modelling methods to explore whether local power spectral differences can account for functional network changes in AD. In the model, local dynamics are described by natural frequencies whilst coupling is described by the effective connectivity (EC). (A) The natural frequency distribution for each subject was given for each ROI by the frequency with peak power in the 6–13 Hz band in the data. (B) A representative EC was used for all subjects, generated as follows. The natural frequencies of each ROI were given by their median value from the HOA subjects. EC was optimized using an iterative algorithm (see methods) in order to replicate the median HOA FC. (C) For each subject, time series were simulated using individual natural frequencies and the template EC. Comparisons can then be made between HOA and AD simulations to test whether changes to local dynamics explain FC differences in the data.

all 47 subjects with global coupling adjusted. The resulting estimates of global coupling strength were smaller in the AD cohort, though not significantly different from the HOA (Fig. 8B, HOA = 4.12 ± 0.45, AD = 2.91 ± 0.53; $p = 0.1016$). This supports the disconnection hypothesis of AD, since lower global coupling strength was required in the AD cohort to recreate the observed differences in FC mean degree.

In the simulated functional networks, small-worldness was found to decrease, but not significantly ($p = 0.0502$), in AD compared to HOA. However, we examined the spatial distribution of changes to closeness centrality in AD compared to HOA, and found

this did not replicate the subject data. For example, in the subject data, the largest effect sizes were found in the temporal lobes, whilst simulated networks exhibited large effect sizes in the right frontal, temporal, and parietal lobes (Fig. 9A, Table S4). Therefore, we found that changes to the intrinsic dynamics alone, via the incorporation of the distribution of intrinsic frequencies across nodes, was not sufficient to describe topological changes to the functional network; particularly increased path lengths in the temporal lobes. This suggested that alterations to the effective connectivity would be required in order for the model to fully explain the data.
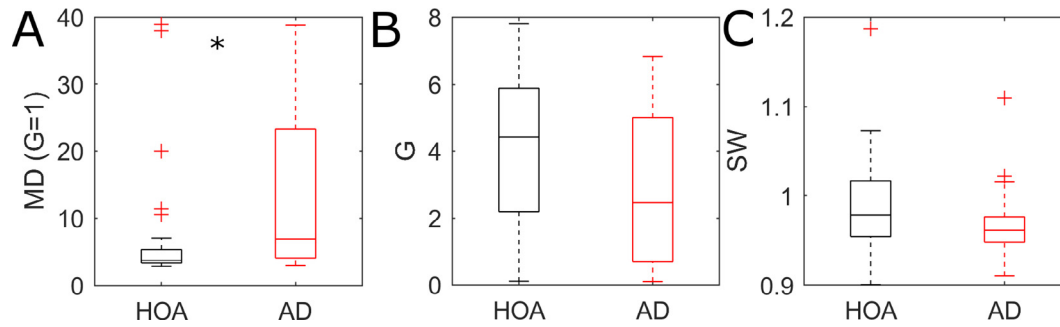
Fig. 8. Comparisons of HOA and AD in simulated functional networks. (A) Initially, networks were simulated with the same effective connectivity, with the only differences between subjects in the model was the natural frequency of the Hopf oscillators, set to the subject specific power spectral peak frequency. Mean degree of these networks significantly increased. (B) Global coupling strength in the networks was then altered such that the mean degree of a given subject's simulated network equaled the mean degree of the subject's empirical network. G was found to decrease non-significantly. (C) Small worldness does not significantly decrease in the simulated networks, however, the effect size of the decrease is large ($p = 0.0507$).
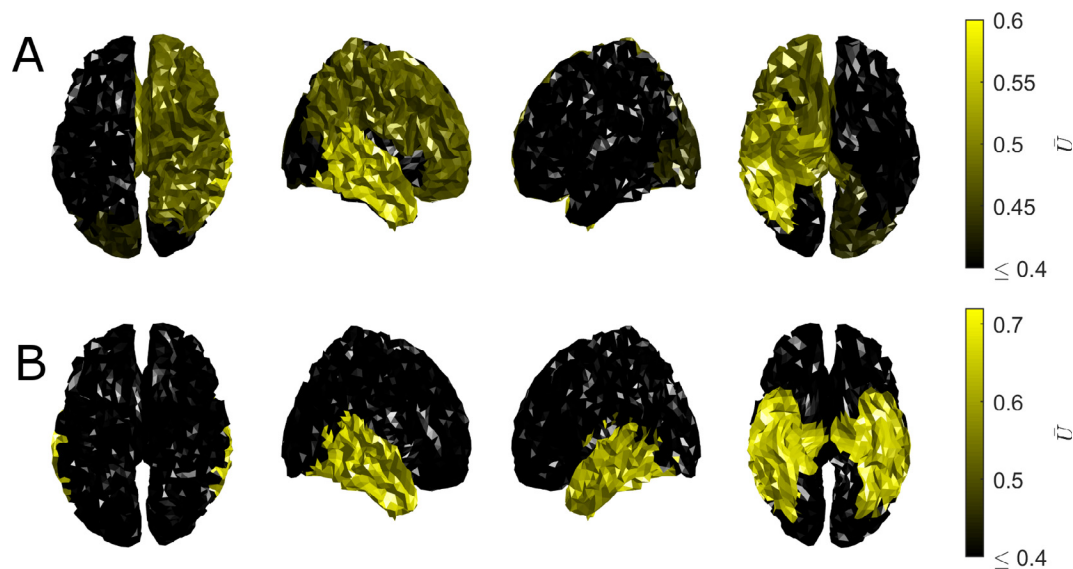

Fig. 9. In the simulated networks, temporal lobe disconnection is required for similar spatial distributions of changes in closeness to the data. (A) Effect sizes of closeness centrality in simulated networks (no temporal lobe disconnection). The largest effect sizes for changes in closeness centrality were found in the frontal, parietal, and temporal lobes. (B) Effect sizes of closeness centrality in simulated networks (with temporal lobe disconnection). The largest effect sizes were found in the two temporal lobes, which more accurately represents the results seen in the data.

To test this, we simulated a reduction in temporal lobe connectivity by multiplying all effective connections to ROIs in the temporal lobes by a constant $0 \leqslant \alpha < 1$. We simulated the model for a range of values of α and found that the spatial distributions of changes in closeness centrality in AD networks demonstrated large effect sizes constrained to the temporal lobes, therefore closely replicating the data. Fig. 9B and Table S4 demonstrate these results for $\alpha = 0.5$. Simulations over a range of values of α showed consistency in the results, particularly for $\alpha < 0.8$ (Fig. S5). These results suggest that the observed changes in functional connectivity are due to reduced effective connectivity (likely due to loss of synaptic connectivity) between the temporal lobes and the rest of the brain, combined with alterations to the intrinsic frequencies of oscillations within nodes.

4. Discussion

In this work, EEG and cognitive test scores from AD and HOA subjects were analysed in order to explore how disruptions to connectivity in the brain and altered local dynamics relate to cognitive deficits. We found that whilst significant alterations to the power spectrum and average synchrony between regions of the brain were identified, these were not indicators of the level of cognitive decline in AD patients. However, topological organization of the networks, as quantified by small-worldness, was found to significantly and positively correlate with MMSE score, particularly the language sub-score. Reduced small-worldness was found to be driven predominantly by reduced closeness of the temporal lobes, which computational modelling suggests was likely driven by impaired synaptic connectivity between the temporal lobes and other regions, in combination with heterogeneous spectral slowing. These results give potential insight into the role that disruption to temporal lobe connectivity plays in language impairments in AD, and more generally advances our understanding of how the disconnection hypothesis of AD relates to the phenotype of the disease.

4.1. Methodology

A major methodological difference between the study presented here and the majority of previous EEG studies in AD is that the EEG presented here was recorded in an eyes open, as opposed to an eyes closed state. It has been shown that both the power spectrum and functional networks are different in eyes open and eyes closed conditions (Wu et al., 2010; Tan et al., 2013; Miraglia

et al., 2016; Kan et al., 2017). Therefore our work provides insight into a different active network than the large literature on EEG in AD recorded in eyes closed resting state conditions (Strik et al., 1997; Adler et al., 2003; Lindau et al., 2003; Dauwels et al., 2011; Hatz et al., 2015; Wang et al., 2015; Liu et al., 2015; Goossens et al., 2017; Ianof et al., 2017). Since cognitive deficits in AD predominantly relate to the awake and alert states, it is possible that studying eyes open data gives key insight into how network deficits drive cognitive decline. This could underpin our finding that network small-worldness correlated with MMSE score in the AD cohort, whereas previous studies conducted in the eyes closed paradigm found no such correlations in both EEG and fMRI (Stam et al., 2007; Sanz-Arigita et al., 2010). An additional key strength of the data used in this study is that all patients were free from dementia related medications, meaning the results presented here can not be an artifact of medication induced alterations to network states.

Another methodological step taken was to map the EEG into source space. Source space analyses have the advantage of being able to attribute activity to specific regions of the brain, thereby allowing for anatomical interpretation of the results (Michel et al., 2004). This is particularly useful when studying neurological disorders, as it allows for study of the spatial distribution of neuropathology. However, the method of source mapping we used relies on a number of key assumptions. Firstly, a simplifying assumption in building the forward model was to consider the head as being constructed of three homogeneously conducting layers of tissue (Fuchs et al., 2002; Oostenveld et al., 2003). Secondly, we worked with the assumption that a template head model would provide a sufficient mapping for all patients. A range of methods for building the forward model, from a single homogeneously conducting sphere to highly detailed, realistic models containing many layers of anisotropically conducting tissue, are available (Hallez et al., 2007), but a trade-off between computational expense and accuracy of the results must be made when deciding on a method to generate a forward model. In the absence of individual MRI scans, the three (homogeneous and isotropic) layer boundary element method template head model used in this study has been shown to perform to a much higher standard than a three layer spherical head model and to a comparable level as individually derived three layer head models (Fuchs et al., 2002). Furthermore, boundary-element method models are reasonably computationally inexpensive (Hallez et al., 2007). For these reasons, there is a trend in studies such as ours where individual MRIs are unavailable, to use a template head model consisting of three homogeneously and isotropically conducting layers (Cantero et al., 2009; Canuet et al., 2011; Aoki et al., 2015; Hata et al., 2016; Ianof et al., 2017; Ikeda et al., 2017; Vecchio et al., 2017; Smith et al., 2018; Medvedeva and Yanho, 2018; Farina et al., 2018). It is, however, unclear to what extent the effect of aging and potential cortical atrophy in AD patients may have on the validity of this template head model. Nonetheless, there exists much precedent for use of a template head model in studies concerning older adults and AD patients (Canuet et al., 2012; Vecchio et al., 2014, 2017; Hata et al., 2016; Ianof et al., 2017; Medvedeva and Yanho, 2018). For AD patients, data was recorded within days of diagnosis, and so whilst severe cortical atrophy is unlikely, this cannot be ruled out without validation using an MRI. Regardless, because of the use of a template head model that may not capture individual differences, changes in head shape due to aging, and the fact we cannot rule out the presence of atrophy, all statistical analyses were performed on the level of lobes of the brain, meaning results are likely to be robust to small errors in localization.

Furthermore, the functional networks derived from the source space data are dependent on the combination of reconstruction method and functional connectivity method (Hassan et al., 2014; Hassan et al., 2017; Finger et al., 2016). Here, our choice of eLORETA was motivated by desire to map 64 channel EEG to large-scale source dynamics (see e.g. Schirner et al., 2015; Finger et al., 2016). Estimation of spatially smooth current source density by inverse modelling is dependent on the number of electrodes used (Hassan et al., 2017); due to discrete sampling of electrodes on the scalp, the information that can be used to describe source dynamics is limited by the number of electrodes. For studies with a similar number of electrodes to the one presented here (60–71 electrodes) eLORETA has been demonstrated to outperform other linear inverse methods such as minimum norm estimates and linearly constrained minimum variance at localizing sources and network estimation in studies with known source origin such as simulations (Pascual-Marqui et al., 2011; Finger et al., 2016), deep brain stimulation (Mideksa et al., 2016), and comparisons of resting state networks with fMRI (Liu et al., 2018), further motivating our use of the eLORETA algorithm to perform source reconstruction. The choice of PLF was motivated by simulations demonstrating the eLORETA/PLF combination could accurately recreate ground truth functional connectivity matrices (Finger et al., 2016). Since eLORETA incorporates spatial smoothness constraints, neighbouring source points will demonstrate strong instantaneous correlations (Pascual-Marqui et al., 2011). To mitigate these source leakage effects zero-lag PLF values were disregarded in our study (Schmidt et al., 2014).

A methodological point of note in this study is the use of 20 s of data. Typically, EEG studies use epoch lengths of the order seconds to minutes (Gudmundsson et al., 2007). For epoch lengths of these orders of magnitude, studies of spectral measures have found little information to be gained from using epochs longer than approximately 20 s (Gasser et al., 1985; Salinsky et al., 1991; Gudmundsson et al., 2007), whilst studies of small-worldness properties of functional networks derived from phase measures have demonstrated reliability at around 6 s epoch length (Fraschini et al., 2016). However, it is worth noting that long term EEG, intracranial, and simulation studies have demonstrated that over periods of hours and days there are fluctuations in functional network measures (Honey et al., 2007; Kunhert et al., 2010; Chu et al., 2012) such as small-worldness derived from phase locking networks (Kunhert et al., 2010).

4.2. Electrophysiological and network markers of Alzheimer's Disease

Power spectral slowing in the EEG of AD patients has been established for over 20 years (Strik et al., 1997), and has been consistently identified as increases in low frequency power (Strik et al., 1997; Adler et al., 2003; Lindau et al., 2003; Dauwels et al., 2011; Hatz et al., 2015; Liu et al., 2015; Wang et al., 2015), decreases in high frequency power power (Strik et al., 1997; Lindau et al., 2003; Dauwels et al., 2011; Liu et al., 2015; Wang et al., 2015), and reduced peak frequency (Goossens et al., 2017). Our power spectral results were largely consistent with this literature, particularly identifying increases in the contributions of slow (theta) rhythms and reductions to peak power spectral frequency. However, many of these past studies were performed in sensor space, therefore very few studies have identified regions of the brain responsible for this power spectral slowing, information which may potentially be insightful for the development of treatments and understanding disease progression. In this study, increases in the relative power of slow oscillatory activity was localized to the frontal and parietal lobes, which is largely in agreement with the results of Ianof et al. (2017). Interestingly, we found no correlation between theta band relative power and cognition as measured by MMSE. Engels et al. (2016) also found cortical theta power did not correlate with MMSE score in AD patients, but

source reconstructed hippocampal theta power did. This suggests that while we found no correlation between slowing and MMSE scores, this could be due to our restricting source space to the cortical surface.

Disconnection between regions of the brain is believed to play an important role in cognitive decline in AD (Delbeuck et al., 2003). An EEG marker of this is reduced synchrony between regions of the brain (Adler et al., 2003; Pijnenburg et al., 2008; Wang et al., 2014, 2015; Hata et al., 2016). However, in this study and others (Koenig et al., 2005; Gallego-Jutgla et al., 2015; Cantero et al., 2009), increases in functional connectivity were identified in AD, here quantified by a significantly increased weighted mean degree. It is possible that these inconsistencies are due to variations in methodology; choice of functional connectivity and use of weighted or unweighted networks can result in differences in the functional network structure, topology, and sensitivity to changes in AD (Dauwels et al., 2010; Joudaki et al., 2012; Jalili, 2016). Important to note, however, is that the increased mean degree may not be in opposition to the disconnection hypothesis; using computational modelling, we found that changes in mean degree (as well as localized changes in degree) were well explained by intrinsic changes in dynamics, namely power spectral slowing (Fig. S6). In fact, to accurately recreate mean degrees on a subject-by-subject basis, global coupling strength decreased (albeit non-significantly) in AD, suggestive of global disconnection. The slowing itself may also be evidence for disconnection in AD, since modelling studies have suggested power spectral slowing may arise from disconnection between the cortex and thalamus (Abuhassan et al., 2014) identified in fMRI studies (Wang et al., 2012). Changes in mean degree did not correlate with cognitive test scores, which may also be supportive of the hypothesis that power spectral changes are driving the differences in MD since power spectral differences showed no correlation to MMSE.

Small-worldness was used as a measure of network topology (Humphries and Gurney, 2008), since a small-world network is structured for efficient information transfer on both a local and global scale (Watts and Strogatz, 1998; Latora and Marchiori, 2001), and small-worldness of the functional network has consistently been reported to reduce in AD (Stam et al., 2007; de Hann et al., 2009; Wang et al., 2014; Vecchio et al., 2017). Our results were in line with this past literature, finding that smallworldness was reduced in the AD cohort. Furthermore, we found that the reduction in small-worldness was driven by an increased characteristic path length, which is also in line with previous literature (Stam et al., 2007; Vecchio et al., 2014). To understand better how these changes arose, closeness centrality of each node (which is a local counterpart to the inverse of characteristic path length) was calculated, and found to decrease in the temporal lobes, suggesting that increased path lengths in the temporal lobes are likely highly important for the changes in global network topology seen in AD. Furthermore, small-worldness was found to significantly correlate with MMSE score in the AD cohort, which suggests that network topology, as opposed to the amount of synchrony in the network, is highly important for cognition and is likely a key driver of cognitive deficits in AD.

Many more recent studies tend to use efficiency based measures instead of small-worldness (Berlot et al., 2016; Afshari and Jalili, 2017; Sami et al., 2018). Global efficiency is strongly related to the characteristic path length of the network, but is more sensitive to changes in short paths (Rubinov and Sporns, 2010), and is a measure of how efficiently information can be transferred through the network on average (Latora and Marchiori, 2001). The local counterpart to global efficiency, local efficiency, performs a similar function to the clustering coefficient (Latora and Marchiori, 2001), describing how efficiently neighbours of a given node are connected. Local efficiency has been suggested to be highly suitable

for examining the effect of neurodegenerative syndromes such as AD (Sami et al., 2018), since the local efficiency quantifies the tolerance of the network to dysfunction at that node (Latora and Marchiori, 2001; Rubinov and Sporns, 2010). Small-worldness is related to local and global efficiency in that a small-world network has both high local and global efficiencies (Latora and Marchiori, 2001). For these reasons, we also ran the topological analysis with global and local efficiency replacing small-worldness and closeness, and found that trends were similar in the efficiency analysis but effect sizes were generally smaller (see Supplementary Text S1). Importantly, this allows us to interpret our results in terms of information transfer in the network, suggesting that in AD the temporal lobes play less of a role in aiding the flow of information through the brain than in HOA. This, combined with the highly related increased closeness, suggest that the temporal lobes are becoming functionally less integrated with the rest of the brain in AD.

A computational model based on that of Dermitas et al. (2017) was used to explore the mechanisms underpinning functional network differences in the AD cohorts. Dermitas et al. (2017) used individual structural MRIs to derive initial EC matrices for the iterative optimization algorithm. It was therefore reasonable to assume the optimized EC is representative of synaptic EC, and to use these to make inferences on changes of the structure of the brain in AD. In this study, a template, unweighted structural MRI was used for initial EC, and hence the simple iterative algorithm used for optimization is unlikely to give a global optimum. Hence, we do not aim to interpret the EC matrices derived here as representative of structural differences between regions of the brain. Instead, the only interpretation we make is that the effective connectivity matrices are sufficient to generate realistic functional connectivity. For this reason, all analyses of the model output are related to the simulated functional connectivity, and we do not analyse individual effective connectivity in a similar manner to Dermitas et al. (2017). That said, the effective connectivity presented here can still give important insight into how effective connectivity changes in AD. Our modelling results suggest that given a generative model of HOA functional connectivity, alterations to long range effective connections in the temporal lobe are required to cause functional connectivity representative of the AD cohort.

A key assumption of the modelling procedure is that power spectral differences are intrinsic to regions of interest and not a result of altered connectivity. Whilst the accuracy of this assumption is unclear, provided we view the model as a way to generate realistic functional connectivity patterns and not a biophysically realistic representation of neuronal activity, this assumption does not alter the results. However, it is important that we interpret results such as those shown in Fig. 8 and Fig. S6 as showing that intrinsic power spectral differences are a potential and sufficient mechanism to drive certain changes to functional connectivity in AD, but without further experimental evidence we can not know whether this is the true mechanism. Regardless, this does not change the key result presented here, which demonstrates that even intrinsic power spectral changes would not be sufficient to drive the changes in small-worldness and closeness observed in the data, and that further synaptic mechanisms (such as temporal lobe disconnection) are required.

Whilst other neurodegenerative disorders or dementia aetiologies were not examined in this study, the methods used here are likely to be applicable. Spectral slowing and functional network alterations have been reported in vascular dementia (Neto et al., 2015; van Straaten et al., 2015), dementia with Lewy bodies (Kai et al., 2005; Andersson et al., 2008; Bonnani et al., 2008; Roks et al., 2008; Dauwan et al., 2016), and frontotemporal lobar degeneration (Lindau et al., 2003; de Hann et al., 2009; Yu et al., 2016; Sami et al., 2018). Many of these studies have found differences

in the sensor space topography of spectral and network alterations than can discriminate between AD and other types of dementia (Bonnani et al., 2008; Nishida et al., 2011; Neto et al., 2015; Dauwan et al., 2016; Yu et al., 2016; Sami et al., 2018), but very few have applied source space reconstruction (Nishida et al. (2011) being a notable exception) to study the spatial differences in terms of cortical generators. Therefore it would be of interest for future work to apply the source space and computational modelling approaches used here to study other dementias.

4.3. Temporal lobe disconnection, phenotype, and the potential role of tau pathology

In this paper, we augmented our functional network study with computational modelling and correlation with cognitive test scores. This allowed us to relate functional network changes with pathological mechanisms, and increase our understanding of how specific network disruptions can drive exact cognitive deficits characteristic of AD.

Small-worldness of the functional network was found to significantly correlate with both total MMSE score and the language subscore, suggesting topology of the functional network plays a key role in driving language deficits in early stage AD. Local graph theoretical analysis and computational modelling suggested that changes in small-worldness were a result of long range structural and functional disconnection in the temporal lobes. Language impairment in AD has previously found to be linked to temporal lobe atrophy in structural MRI, functional MRI, SPECT, PET, CT and post-mortem studies (Harasty et al., 1999; Galton et al., 2000; Domoto-Reilly et al., 2012), and language impairments have been linked to neuronal death and functional connectivity in the temporal lobe in other neurological disorders such as temporal lobe epilepsy (Bartha et al., 2005; Trimmel et al., 2018). Whilst past studies in AD have identified temporal lobe network deficiencies in both functional (Medvedeva and Yanho, 2018; Canuet et al., 2012) and effective networks (Dermitas et al., 2017), this is the first study the authors are aware of that have complemented this with cognitive test scores and found a direct link with language deficiencies in AD.

The pathological mechanisms driving the effective connectivity, functional connectivity, and cognitive changes reported here are still unclear, but we hypothesise tau pathology plays a critical role. AD has two primary pathologies, namely amyloid plaques and neurofibrillary tangles due to hyperphosphorlyated tau protein (Querfurth and LaFerla, 2010). In AD, tau pathology originates in and around the temporal cortex (Braak and Braak, 1991), and temporal lobe tau pathology has consistently been reported in patients with AD in both post-mortem and neuroimaging studies (Saint-Aubert et al., 2017; Galton et al., 2000). From the EEG, it is not possible to directly measure tau burden in our cohort of patients. However, functional network measures such as closeness centrality and local efficiency have been identified to negatively correlate with tau burden (Cope et al., 2018), meaning interpreting these as a potential proxy for tau burden would suggest temporal lobe tauopathy in our patients. PET imaging has correlated the severity of temporal lobe tau burden with language impairments in AD (Bejanin et al., 2017), whilst post-mortem studies have demonstrated particularly strong tau burden in the temporal cortex of aphasic AD patients (Galton et al., 2000). Therefore, there is much evidence alluding to tauopathy as a pathological driver for the network and cognitive changes reported here. Whilst amyloidopathy is also likely important for cognitive changes in AD, this link appears to be less direct, with many studies finding tau burden correlates more strongly with cognitive test scores than amyloid (Nelson et al., 2012) – more specifically, a PET study found that temporal lobe tau burden correlates with language deficiencies in AD, but temporal lobe amyloid burden does not (Bejanin et al., 2017).

4.4. Summary and conclusions

In this work, we propose long range synaptic disconnection in the temporal lobes as a potential mechanism directly underpinning cognitive and language deficits in AD. The results presented here suggest that this synaptic disconnection manifests itself in the form of reduced effective connectivity between the temporal lobes and other anatomical regions of the brain. This reduced effective connectivity results in reduced functional integration of the temporal lobes and less efficient global network organization (reduced 'small-worldness'), in turn leading to cognitive deficits in the form of language dysfunction. Increased mean degree is also observed in the networks, but computational modelling suggests that this change, unlike the topological network measures, can be well described by heterogeneous power spectral slowing; in fact, global disconnection was required to accurately replicate the mean degree of each network. The results presented here give key insight into a specific link between disconnection, namely functional and effective disconnection of the temporal lobes, and language deficiencies in the early stages of AD. The anatomically localized nature of the findings and links with a specific cognitive domain mean that these results have the potential to inform treatments and therapies for patients diagnosed with Alzheimer's Disease.

Declaration of Competing Interest

None of the authors have potential conflicts of interest to be disclosed.

Appendix A. Supplementary material

Supplementary data associated with this article can be found, in the online version, at https://doi.org/10.1016/j.clinph.2019.05.027.

References

Abuhassan K, Coyle D, Maguire L. Compensating for thalamocortical synaptic loss in Alzheimer's disease. Front Comput Neurosci 2014;8:65.

Adler G, Brassen S, Jajcevic A. EEG coherence in Alzheimer's dementia. J. Neural Transm 2003;110:1051–8.

Afshari S, Jalili M. Directed functional networks in Alzheimer's disease: disruption of global and local connectivity measures. IEEE J Biomed Health Inform 2017;21 (4):949–55.

Agronin M. Alzheimer's disease and other dementias: a practical guide. 3rd ed. Routledge; 2014.

American Psychiatric Association. Diagnostic and statistical manual of mental disorders (IV-TR). Washington DC; 2000.

Andersson M, Hansson O, Minthon L, Rosén I, Londos E. Electroencephalogram variability in dementia with Lewy bodies, Alzheimer's disease and controls. Dement Geriatr Cogn Disord 2008;26:284–90.

Aoki Y, Ishii R, Pascual-Marqui R, Canuet L, Ikeda S, Hata M, et al. Detection of EEG-resting state independent networks by eLORETA-ICA method. Front Hum Neurosci 2015;9:31.

Babiloni C, Lizio R, Marzano N, Capotosto P, Soricelli A, Triggiani A, et al. Brain neural synchronization and functional coupling in Alzheimer's disease as revealed by resting state EEG rhythms. Int J Psychophysiol 2016;103:88–102.

Badhwar A, Tam A, Dansereau C, Orban P, Haffstardter F, Bellec P. Resting-state network dysfunction in Alzheimer's disease: a systematic review and meta-analysis. Alzheimers Dement (Amst) 2017;8:73–85.

Barker W, Luis C, Kashuba A, Luis M, Harwood D, Loewenstein D, et al. Relative frequencies of Alzheimer disease, Lewy body, vascular and frontotemporal dementia, and hippocampal sclerosis in the State of Florida brain bank. Alzheimer Dis Assoc Disord 2002;16(4):203–12.

Bartha L, Benke T, Bauer G, Trinka E. Interictal language functions in temporal lobe epilepsy. J Neurol Neurosurg Psychiatry 2005;76(6):808–14.

Bejanin A, Schonhaut D, La Joie R, Kramer J, Baker S, Sosa N, et al. Tau pathology and neurodegeneration contribute to cognitive impairment in Alzheimer's disease. Brain 2017;140(12):3286–300.

Berlot R, Metzler-Baddeley C, Ikram M, J. DK, O'Sullivan M. Global efficiency of structural networks mediates cognitive control in mild cognitive impairment. Front Aging Neurosci 2016;8:292.

Bermejo-Pareja F, Benito-Leon J, Vega S, Medrano M, Roman Gin Central Spain (NEDICES) Study Group, N.D.. Incidence and subtypes of dementia in three elderly populations of central spain. J Neurol Sci 2008;246(1-2):64–72.

Bonnani L, Thomas A, Tiraboschi P, Perfetti B, Varanese S, Onofrj M. EEG comparisons in early Alzheimer's disease, dementia with Lewy bodies, and Parkinson's disease with dementia patients with a 2-year follow-up. Brain 2008;131(3):690–705.

Braak H, Braak E. Neuropathological stageing of Alzheimer-related changes. Acta Neuropathol 1991;82:239–59.

Brueggen K, Fiala C, Berger C, Ochmann S, Bablioni C, Teipel S. Early changes in alpha band power and DMN BOLD activity in Alzheimer's disease: a simultaneous resting state EEG-fMRI study. Front Aging Neurosci 2017;9:319.

Buzsaki G. Rhythms of the brain. Oxford University Press; 2006.

Cantero J, Atienza M, Cruz-Vadell A, Suarez-Gonzalez A, Gil-Neciga E. Increased synchronization and decreased neural complexity underlie thalamocortical oscillatory dynamics in mild cognitive impairment. NeuroImage 2009;46:938–48.

Canuet L, Ishii R, Pascual-Marqui R, Iwase M, Kurimoto R, Aoki Y, et al. Resting-state EEG source localization and functional connectivity in schizophrenia-like psychosis of epilepsy. PLoS ONE 2011;6(11). e27863.

Canuet L, Tellado I, Courceiro V, Fraile C, Fernandez-Novoa L, Ishii R, et al. Resting-state network disruption and apoe genotype in Alzheimer's disease: a lagged functional connectivity study. PLoS ONE 2012;7(9). e46289.

Chu C, Kramer M, Pathmanathan J, Bianchi M, Westover M, Wizon L, et al. Emergence of stable functional networks in long-term human electroencephalography. J Neurosci 2012;32(8):2703–13.

Cope T, Rittman T, Borchert R, Jones P, Vatansever D, Allinson K, et al. Tau burden and the functional connectome in alzheimer's disease and progressive supranuclear palsy. Brain 2018;141(2):550–67.

Crosson B, Ford A, McGregor K, Meinzer M, Cheshkov S, Li X, et al. Functional imaging and related techniques: an introduction for rehabilitation researchers. J Rehabil Res Dev 2010;47(2):vii–xxxiv.

Cureton E. Rank-biserial correlation. Psychometrika 1956;21(3):287–90.

Dauwan M, van Dellen E, van Boxtel L, van Straaten E, de Waal H, Lemstra A, et al. EEG-directed connectivity from posterior brain regions is decreased in dementia with Lewy bodies: a comparison with Alzheimer's disease and controls. Neurobiol Aging 2016;41:122–9.

Dauwels J, Srinivasan K, Reddy M, Musha T, Vialatte F, Latchoumane C, et al. Slowing and loss of complexity in Alzheimer's EEG: two sides of the same coin? Int J Alzheimers Dis 2011;2011. 539621.

Dauwels J, Vialatte F, Musha T, Cichocki A. A comparative study of synchrony measures for the early diagnosis of Alzheimer's disease based on EEG. NeuroImage 2010;49:668–93.

de Haan W, van der Flier W, Wang H, Van Mieghem P, Scheltens P, Stam C. Disruption of functional brain networks in Alzheimer's disease: what can we learn from graph spectral analysis of resting state magnetoencephalography? Brain Connect 2012;2(2).

de Hann W, Pijnenburg Y, Strijers R, Made Y, van der Flier W, Scheltens P, et al. Functional neural network analysis in frontotemporal dementia and Alzheimer's disease using EEG and graph theory. BMC Neurosci 2009;10:101.

Delbeuck X, Van der Linden M, Collette F. Alzheimer's disease as a disconnection syndrome? Neuropsychol Rev 2003;13(2):79–92.

Dermitas M, Falcon C, Tucholka A, Gispert J, Molinuevo J, Deco G. A whole-brain computational modeling approach to explain the alterations in resting-state functional connectivity during progression of Alzheimer's disease. NeuroImage: Clin 2017;16:343–54.

Dierks T, Jelic V, Pascual-Marqui R, Wahlund LPJ, Linden D, Maurer K, et al. Spatial pattern of cerebral glucose metabolism (PET) correlates with localization of intracerebral EEG-generators in Alzheimer's disease. Clin Neurophysiol 2000;111:1817–24.

Dijkstra E. A note on two problems in connexion with graphs. Numer Math 1959;1:269–71.

Domoto-Reilly K, Sapolsky D, Brickhouse M, Dickerson B. Naming impairment in Alzheimer's disease is associated with left anterior temporal lobe atrophy. NeuroImage 2012;63(1):348–55.

Engels M, Hillebrand A, van der Flier W, Stam C, Scheltens P, van Straaten E. Slowing of hippocampal activity correlates with cognitive decline in early onset Alzheimer's disease. An MEG study with virtual electrodes. Front Hum Neurosci 2016;10:238.

Fan L, Li H, Zhuo J, Zhang Y, Wang J, Chen L, et al. The human brainnetome atlas: a new brain atlas based on connectional architecture. Cereb Cortex 2016;26 (8):3508–26.

Farina B, Della Marca G, Maestoso G, Amoroso N, Valenti E, Carbone G, et al. The association among default mode network functional connectivity, mentalization, and psycopathology in a nonclinical sample: an eLORETA study. Psychopathology 2018;51:16–23.

Finger H, Bönstrup M, Cheng B, Messé A, Hilgetag C, Thomalla G, et al. Modeling of large-scale functional brain networks based on structural connectivity from DTI: comparison of EEG derived phase coupling networks and evaluation of alternative methods along the modeling path. PLoS Comput Biol 2016;12(8). e1005025.

Folstein M, Folstein S, McHugh P. Mini-mental state. a practical method for grading the cognitive state of patients for the clinician. J Psychiat Res 1975;12:189–98.

Fraschini M, Demuru M, Crobe A, Marrosu F, Stam C, Hillebrand A. The effect of epoch length on estimated EEG functional connectivity and brain network organisation. J Neural Eng 2016;13(3). 036015.

Fuchs M, Kastner J, Wagner M, Hawes S, Ebersole J. A standardized boundary element method volume conductor model. Clin Neurophysiol 2002;113 (5):702–12.

Gallego-Jutgla E, Sole-Casals J, Vialatte F, Dauwels J, Cichocki A. A theta-band EEG based index for early diagnosis of Alzheimer's disease. J Alzheimers Dis 2015;43:1175–84.

Galton C, Petterson K, Xuereb J, Hodges J. Atypical and typical presentations of Alzheimer's disease: a clinical, neuropsychological, neuroimaging and pathological study of 13 cases. Brain 2000;123(3):484–98.

Gambuzza L, Gomez-Gardenes J, Frasca M. Amplitude dynamics favors synchronization in complex networks. Sci Rep 2016;6:24915.

Gasser T, Bächer P, Steinberg H. Test-retest reliability of spectral parameters of the EEG. Electroencephalogr Clin Neurophysiol 1985;60(4):312–9.

Goossens J, Laton J, Van Schependom J, Gielen J, Strufs H, Can Mossevelde S, et al. EEG dominant frequency peak differentiates between Alzheimer's disease and frontotemporal lobal degeneration. J Alzheimers Dis 2017;55:53–8.

Gudmundsson S, Runarsson T, Sigurdsson S, Eiriksdottir G, Johnsen K. Reliability of quantitative EEG features. Clin Neurophysiol 2007;118(10):2162–71.

Hallez H, Vanrumste B, Grech R, Muscat J, De Clercq W, Vergult A, et al. Review on solving the forward problem in EEG source analysis. J Neuroeng Rehabil 2007;4:46.

Harasty J, Halliday G, Kril J, Code C. Specific temporoparietal gyral atrophy reflects the pattern of language dissolution in Alzheimer's disease. Brain 1999;122 (4):675–86.

Hassan M, Dufor O, Merlet I, Berrou C, Wendling F. EEG source connectivity analysis: from denser array recordings to brain networks. PLoS ONE 2014;9(8). e105041.

Hassan M, Merlet I, Mheich A, Kabbara A, Biraben A, Nica A, et al. Identification of interictal epileptic networks from dense-EEG. Brain Topogr 2017;30:60–76.

Hassan M, Wendling F. Electroencephalography source connectivity: toward high time/space resolution brain networks; 2018. <http://arxiv.org/pdf/0710.3341>.

Hata M, Kazui H, Tanaka T, Ishii R, Canuet L, Pascual-Marqui R, et al. Functional connectivity assessed by resting state EEG correlates with cognitive decline of Alzheimer's disease - an eLORETA study. Clin Neurophysiol 2016;127:1269–78.

Hatz F, Hardmeier M, Benz N, Ehrensperger M, Gschwandtner U, Ruegg S, et al. Microstate connectivity alterations in patients with early Alzheimer's disease. Alzheimers Res Ther 2015;7:78.

Honey C, Kötter R, Breakspear M, Sporns O. Network structure of cerebral cortex shapes functional connectivity on multiple time scales. Proc Natl Acad Sci USA 2007;104(24):10240–5.

Honey C, Sporns O, Cammoun L, Gigandet X, Thiran J, Meuli R, et al. Predicting human resting-state functional connectivity. Proc Natl Acad Sci USA 2009;106 (6).

Humphries M, Gurney K. Network small world-ness: a quantitative method for determining canonical network equivalence. PLoS ONE 2008;3(4). e0002051.

Ianof J, Fraga F, Ferreira L, Ramos R, Demario J, Baratho R, et al. Comparative analysis of the electroencephalogram in patients with Alzheimer's disease, diffuse axonal injury patients and healthy controls using LORETA analysis. Dement Neuropsychol 2017;11(2):176–85.

Ikeda S, Ishii R, Canuet L, Pascual-Marqui R. Source estimation of epileptic activity using eLORETA kurtosis analysis. BMJ Case Rep 2017, bcr-2017-222123; 2017.

Jalili M. Functional brain networks: does the choice of dependency estimator and binarization method matter? Sci Rep 2016;6:29780.

Joudaki A, Salehi N, Jalili M, Knyazeva M. EEG-based functional brain networks: does the network size matter? PLoS One 2012;7(4). e35673.

Kai T, Asai Y, Sakuma K, Koeda T, Nakashima K. Quantitative electroencephalogram analysis in dementia with Lewy bodies and Alzheimer's disease. J Neurol Sci 2005;237(1–2):89–95.

Kan D, Croarkin P, Phang C, Lee P. EEG differences between eyes-closed and eyes-open conditions at the resting stage for euthymic participants. Neurophysiology 2017;49(6):432–40.

Klimesch W. EEG alpha and theta oscillations reflect cognitive and memory performance: a review and analysis. Brain Res Rev 1999;29:169–95.

Koenig T, Prichep L, Dierks T, Hubl D, Wahlund L, John E, et al. Decreased EEG synchronization in Alzheimer's disease and mild cognitive impairment. Neurobiol Aging 2005;26(2):165–71.

Kunhert M, Elger C, Lehnertz K. Long-term variability of global statistical properties of epileptic brain networks. Chaos 2010;20. 043126.

Lachaux J, Rodriguez E, Martinerie J, Varela F. Measuring phase synchrony in brain signals. Hum Brain Mapp 1999;8(4):194–208.

Latora V, Marchiori M. Efficient behaviour of small-world networks. Phys Rev Lett 2001;87(19). 198701.

Lindau M, Jelic V, Johansson S, Andersen C, Wahlund L, Almkvist O. Quantitative EEG abnormalities and cognitive dysfunctional in frontotemporal dementia and Alzheimer's disease. Dement Geriatr Cogn Disord 2003;15:106–14.

Liu Q, Ganzetti M, Wenderoth N, Mantini D. Detecting large-scale brain networks using EEG: Impact of electrode density, head modeling and source localization. Front Neuroinform 2018;12:4.

Liu X, Zhang C, Ji Z, Ma Y, Shang X, Zhang Q, et al. Multiple characteristics analysis of Alzheimer's electroencephalogram by power spectral density and lempel-ziv complexity. Cogn Neurodyn 2015;10:121–33.

Lo C-Y, Wang P-N, Chou K-H, Wang J, He Y, Lin C-P. Diffusion tensor tractography reveals abnormal topological organization in structural cortical networks in Alzheimer's disease. J Neurosci 2010;30(50):16876–85.

Lowet E, Roberts M, Peter A, Gips B, De Weerd P. A quantitative theory of gamma synchronization in macaque V1. eLife 2017; 6: e26642.

McKhann G, Drachman D, Folstein M, Katzman R, Price D, Stadlan E. Clinical diagnosis of Alzheimer's disease: report of the NINCDS-ADRDA work group under the auspices of department of health and human services task force on Alzheimer's disease. Neurology 1984;34:939.

Medvedeva A, Yanho N. Functional connectivity as a neurophysiological biomarker of Alzheimer's disease. J Alzheimers Parkinsonism Dement 2018;3(1):023.

Michel C, Murray M, Lantz G, Gonzalez S, Spinelli L, de Peralta R. EEG source imaging. Clin Neurophysiol 2004;115:2195–222.

Mideksa KG, Singh A, Hoogenboom N, Hellriegel H, Krause H, Schnitzler A, et al. Comparison of imaging modalities and source-localization algorithms in locating the induced activity during deep brain stimulation of the stn. In: 2016 38th annual international conference of the IEEE Engineering in Medicine and Biology Society (EMBC). p. 105–8.

Miraglia F, Vecchio F, Bramanti P, Rossini P. EEG characteristics in eyes open versus eyes closed conditions: small world network architecture in healthy aging and age related brain degeneration. Clin Neurophysiol 2016;127:1261–8.

Mito R, Raffelt D, Dhollander T, Vaughan D, Tournier J, Salvado O, et al. Fibre-specific white matter reductions in Alzheimer's disease and mild cognitive impairment. Brain 2018;141:888–902.

Mulert C, Jäger L, Schmitt R, Bussfeld P, Pogarell O, Möller H, et al. Integration of fMRI and simultaneous EEG: towards a comprehensive understanding of localization and time-course of brain activity in target detection. NeuroImage 2004;22:83–94.

Nelson P, Alafuzoff I, Bigio E, Bouras C, Braak H, Cairns N, et al. Correlation of Alzheimer disease neuropathologic changes with cognitive status: a review of the literature. J Neuropathol Exp Neurol 2012;71(5):362–81.

Neto E, Allen E, Aurlien H, Nordby H, Eichele T. EEG spectral features discriminate between Alzheimer's and vascular dementia. Front Neurol 2015;6:25.

Nishida K, Yoshimura M, Isotani T, Yoshida T, Kitaura Y, Saito A, et al. Differences in quantitative EEG between frontotemporal dementia and Alzheimer's disease as revealed by LORETA. Clin Neurophys 2011;122(9):1718–25.

Olbrich S, Mulert C, Karch S, Trenner M, Leicht G, Pogarell O, et al. EEG-vigilance and BOLD effect during simultaneous EEG/fMRI measurement. NeuroImage 2009;45 (2):319–32.

Olejniczak P. Neurophysiologic basis of EEG. J Clin Neurophysiol 2006;23:186–9.

Oostenveld R, Fries P, Maris E, Schoffelen J. Fieldtrip: Open source software for advanced analysis of MEG, EEG, and invasive electrophysiological data. Comput Intell Neurosci 2011;2011. 156869.

Oostenveld R, Stegeman D, Praamstra P, van Oosterom A. Brain symmetry and topographic analysis of lateralized event-related potentials. Clin Neurophysiol 2003;114(7):1194–202.

Pascual-Marqui R. Discrete, 3d distributed, linear imaging methods of electric neuronal activity. Part 1: Exact, zero error localization; 2007. <http://arxiv.org/pdf/0710.3341>.

Pascual-Marqui R. Theory of the EEG inverse problem. In: Tong S, Thakor N, editors. Quantitative EEG analysis: methods and clinical applications. Boston: Artech House; 2009. p. 121–40.

Pascual-Marqui R, Lehmann D, Koukkou M, Kochi K, Anderer P, Saletu B, et al. Assessing interactions in the brain with exact low-resolution electromagnetic tomography. Phil Trans R Soc A 2011;369:3768–84.

Perneger T. What's wrong with bonferroni adjustments. BMJ 1998;316 (7139):1236–8.

Pijnenburg Y, Strijers R, Made Y, van der Flier W, Scheltens P, Stam C. Investigation of resting-state EEG functional connectivity in frontotemporal lobar degenerations. Clin Neurophysiol 2008;119:1732–8.

Pizzagalli D, Oakes T, Fox A, Chung M, Larson C, Abercrombie H, et al. Functional but not strucutral subgenual prefrontal cortex abnormalities in melancholia. Mol Psychiatry 2004;9:393–405.

Querfurth H, LaFerla F. Alzheimer's disease. N Engl J Med 2010;32(4):329–44.

Roks G, Korf E, van der Flier W, Scheltens P, Stam C. The use of EEG in the diagnosis of dementia with Lewy bodies. J Neurol Neurosurg Psychiatry 2008;79:377–80.

Rose S, Chen F, Chalk J, Zelaya F, Strugnell W, Benson M, et al. Loss of connectivity in Alzheimer's disease: an evaluation of white matter tract integrity with colour coded MR diffusion tensor imaging. J Neurol Neurosurg Psychiatry 2000;69 (4):528–30.

Rubinov M, Sporns O. Complex network measures of brain connectivity: uses and interpretations. NeuroImage 2010;52:1059–69.

Saint-Aubert L, Lemoine L, Chiotis K, Leuzy A, Rodriguez-Vieitez E, Nordberg A. Tau PET imaging: present and future directions. Mol Neurodegener 2017;12:19.

Salinsky M, Oken B, Morehead L. Test-retest reliability in EEG frequency analysis. Electroencephalogr Clin Neurophysiol 1991;79(5):382–92.

Sami S, Williams N, Hughes L, Cope T, Rittman T, Coyle-Gilchrist I, et al. Neurophysiological signatures of Alzheimer's disease and frontotemporal lobar degeneration: pathology vs phenotype. Brain 2018;141:2500–10.

Sanz-Arigita E, Schoonheim M, Damoiseaux J, Rombouts S, Maris E, Barkhof F, et al. Loss of 'small-world' networks in Alzheimer's disease: graph analysis of fMRI resting-state functional connectivity. PLoS ONE 2010;5(11). e13788.

Schirner M, Rothmeier S, Jirsa VKRMA, Ritter P. An automated pipeline for constructing personalized virtual brains from multimodal neuroimaging data. NeuroImage 2015;117:343?357.

Schmidt H, Petkov G, Richardson M, Terry J. Dynamics on networks: the role of local dynamics and global networks on the emergence of hypersynchronous neural activity. PLoS Comput Biol 2014;10(11). e1003947.

Schreiber T, Schmitz A. Improved surrogate data for nonlinearity tests. Phys Rev E 1996;77(4):635–8.

Smith E, Cavanagh J, Allen J. Intracranial source activity (eLORETA) related to scalp-level asymmetry scores and depression status. Psychophysiology 2018;55(1).

Stam C, de Haan W, Daffertshofer A, Jones B, Manshanden I, van Cappellen van Walsum A, et al. Graph theoretical anlaysis of magnetoencephalographic functional connectivity in Alzheimer's disease. Brain 2009;132(1):213–24.

Stam C, Jones B, Nolte G, Breakspear M, Scheltens P. Small-world networks and functional connectivity in Alzheimer's disease. Cereb Cortex 2007;17(1):92–9.

Strik W, Chiaramonti R, Muscas G, Paganini M, Mueller T, Fallgatter A, et al. Decreased EEG microstate duration and anteriorisation of the brain electrical fields in mild and moderate dementia of the Alzheimer type. Psychiatry Res Neuroimag 1997;75:183–91.

Tan B, Kong X, Yang P, Jin Z, Li L. The difference of brain functional connectivity between eyes-closed and eyes-open using graph theoretical analysis. Comput Math Methods Med 2013;2013. 976365.

Trimmel K, van Graan A, Caciagli L, Haag A, Koepp M, Thompson P, et al. Left temporal lobe language network connectivity in temporal lobe epilepsy. Brain 2018;141(8):2406–18.

Tsang A, Lebel C, Bray S, Goodyear B, Hafeez M, Sotero R, et al. White matter structural connectivity is not correlated to cortical resting-state functional connectivity over the healthy adult lifespan. Front Aging Neurosci 2017;9:144.

Uhlhaas P, Singer W. Neural synchrony in brain disorders: relevance for cognitive dysfunctions and pathophysiology. Neuron 2006;52(1):155–68.

van Straaten E, den Haan J, de Waal H, van der Flier W, Barkhof F, Prins N, et al. Disturbed phase relations in white matter hyperintensity based vascular dementia: an EEG directed connectivity study. Clin Neurophys 2015;126 (3):497–504.

Vecchio F, Miraglia F, Marra C, Quaranta D, Vita M, Bramanti P, Rossini P. Human brain networks in cognitive decline: a graph theoretical analysis of cortical connectivity from EEG data. J Alzheimers Dis 2014;41:113–27.

Vecchio F, Miraglia F, Piludu D, Granata G, Romanello R, Caulo M, et al. Small-world artchitecture in brain connectivity and hippocampal volume in Alzheimer's disease: a study via graph theory from EEG data. Brain Imag Behav 2017;11:473–85.

Vitacco D, Brandeis D, Pascual-Marqui R, Martin E. Correspondence of event-related potential tomography and functional magnetic resonance imaging during language processing. Hum Brain Mapp 2002;17:4–12.

Wang R, Wang J, Yu H, Wei X, Yang C, Deng B. Decreased coherence and functional connectivity of electroencephalograph in Alzheimer's disease. Chaos 2014;24. 033136.

Wang R, Wang J, Yu H, Wei X, Yang C, Deng B. Power spectral density and coherence analysis of Alzheimer's EEG. Cogn Neurodyn 2015;9:291–304.

Wang Z, Jia X, Liang P, Qi Z, Yang Y, Zhou W, et al. Changes in thalamus connectivity in mild cognitive impairment: evidence from resting state MRI. Eur J Radiol 2012;81:277–85.

Watts D, Strogatz S. Collective dynamics of 'small-world' networks. Nature 1998;393:440–2.

Wendt D. Dealing with a common problem in social science: a simplified rank-biserial coefficient of correlation based on the u statistic. Eur J Soc Psychol 1972;2(4):463–5.

Wu L, Eichele T, Calhoun V. Reactivity of hemodynamic responses and functional connectivity to different states of alpha synchrony: a concurrent EEG-fMRI study. NeuroImage 2010;52(4):1252–60.

Wu X, Li R, Fleisher A, Reiman E, Chen K, Yao L. Altered default mode network connectivity in Alzheimer's disease – a resting functional MRI and bayesian network study. Hum Brain Mapp 2011;32(11):1868–81.

Yu M, Gouw A, Hillebrand A, Tijms B, Stam C, van Straaten E, et al. Different functional connectivity and networks topology in behavioural variant of frontotemporal dementia and Alzheimer's disease: an EEG study. Neurobiol Aging 2016;42:150–62.

Zumsteg D, Friedman A, Wieser H, Wennberg R. Propogation of interictal discharges in temporal lobe epilepsy: correlaiton of spatiotemporal mapping with intracranial foramen ovale electrode recordings. Clin Neurophys 2006;117:2615–26.

Zumsteg D, Wennberg RA, Treyer V, Buck A, Wieser HG. H2(15)O or 13NH3 PET and electromagnetic tomography (LORETA) during partial status epilepticus. Neurology 2005;65(10):1657–60.